Journal of Materials Chemistry C

ROYAL SOCIETY OF CHEMISTRY

COMMUNICATION

View Article Online
View Journal | View Issue

Cite this: J. Mater. Chem. C, 2021, 9, 10689

Received 6th March 2021,
Accepted 25th June 2021

DOI: 10.1039/d1tc01048d

rsc.li/materials-c

Observation of the correlation between the phonon frequency and long-range magnetic ordering on a MnW octacyanide molecule-based magnet†

Hiroko Tokoro, *[ab] Naotaka Maeda,[a] Kenta Imoto, [b] Koji Nakabayashi, [b] Kouji Chiba[c] and Shin-ichi Ohkoshi *[b]

We show an anomalous change in the phonon frequency at the magnetic phase transition on a cyanide-bridged bimetal assembly, $Mn_3[W(CN)_8]_2(pyrimidine)_4{\cdot}6H_2O$. This compound shows a frequency shift in the CN stretching mode below the magnetic phase transition temperature (T_C). First-principles phonon mode calculation and molecular orbital calculation suggest that the frequency shift of the CN stretching mode is due to the competition of the magnetic energy and the elastic energy. This work demonstrates that a specific change in the phonon frequency is induced by long-range magnetic ordering in flexibly structured matter.

Introduction

Molecule-based magnets, which are composed of metal ions and ligands, are attractive from the viewpoints of rational molecular design and various functionalities.[1–16] In molecule-based magnets, the influence of long-range magnetic ordering such as ferromagnetic (or ferrimagnetic) ordering on the phonon mode is of high interest. Structural flexibility due to the phonon mode in molecule-based magnets should allow changes in the physical properties when a magnetic phase transition occurs.[17] From this viewpoint, we focus on a cyanide-bridged bimetal assembly[18–47] as an example of a molecule-based magnet.[48–53] This is a useful system owing to its various elastic interactions from the stretching modes, transverse translational modes, and transverse librational modes of the cyanide ligand.[26–28] Due to such elastic interactions (phonon modes), the cyanide ligand plays a spring-like role in the cyanide-bridged bimetal assembly. To date, this structural flexibility has realized various types of structural phase transitions, including spin-crossover, charge-transfer, photo-induced, and electric-field-induced phase transitions.[29–47]

Herein we show an anomalous change in the cyanide-stretching phonon mode at the magnetic phase transition, a correlation between the phonon frequency and long-range magnetic ordering, on an octacyanide-bridged manganese tungstate bimetal assembly.

Materials and methods

Materials

The cyanide-bridged manganese tungstate bimetal assembly was prepared using the reported synthesis method.[54] Adding a 5.0 mL aqueous solution of $MnCl_2{\cdot}4H_2O$ (0.20 mol dm^{-3}) to a 5.0 mL aqueous solution of $Cs_3[W(CN)_8]{\cdot}2H_2O$[55] (0.14 mol dm^{-3}) and a 0.1 mL aqueous solution of pyrimidine (1.35 mmol dm^{-3}), yielded a dark brown microcrystal. Elemental analyses of the obtained powder sample showed that the formula was $Mn_3[W(CN)_8]_2(pyrimidine)_4{\cdot}6H_2O$[56] (MnW); calculated: Mn, 11.91; W, 26.30; C, 27.97; N, 24.41; H, 2.10%: found; Mn, 12.17; W, 26.21; C, 28.04; N, 24.34; and H, 2.21%.

Physical measurements

Elemental analyses for Mn and W were performed by an Agilent 7700x inductively coupled plasma mass spectroscopy, and for C, H, and N were performed by standard microanalytical methods. The magnetic properties were measured using a superconducting quantum interference device (SQUID) magnetometer (Quantum Design; MPMS-XL). Single crystal X-ray diffraction measurements at room temperature were performed

[a] Department of Materials Science, Faculty of Pure and Applied Sciences, University of Tsukuba, 1-1-1 Tennodai, Tsukuba, Ibaraki 305-8573, Japan. E-mail: tokoro@ims.tsukuba.ac.jp
[b] Department of Chemistry, School of Science, The University of Tokyo, 7-3-1 Hongo, Bunkyo-ku, Tokyo 113-0033, Japan. E-mail: ohkoshi@chem.s.u-tokyo.ac.jp
[c] Material Science Div., MOLSIS Inc., 3-19-9 Hatchobori, Chuo-ku, Tokyo 104-0032, Japan

† Electronic supplementary information (ESI) available: Results of IR spectrum at room temperature, crystallographic data, TGA data, powder XRD pattern and Rietveld analysis, magnetic properties, IR spectra and peak separation, phonon dispersions, partial phonon density of states obtained by first-principles phonon mode calculations, and far-IR spectra at 12 K and 60 K. CCDC 2061511. For ESI and crystallographic data in CIF or other electronic format see DOI: 10.1039/d1tc01048d

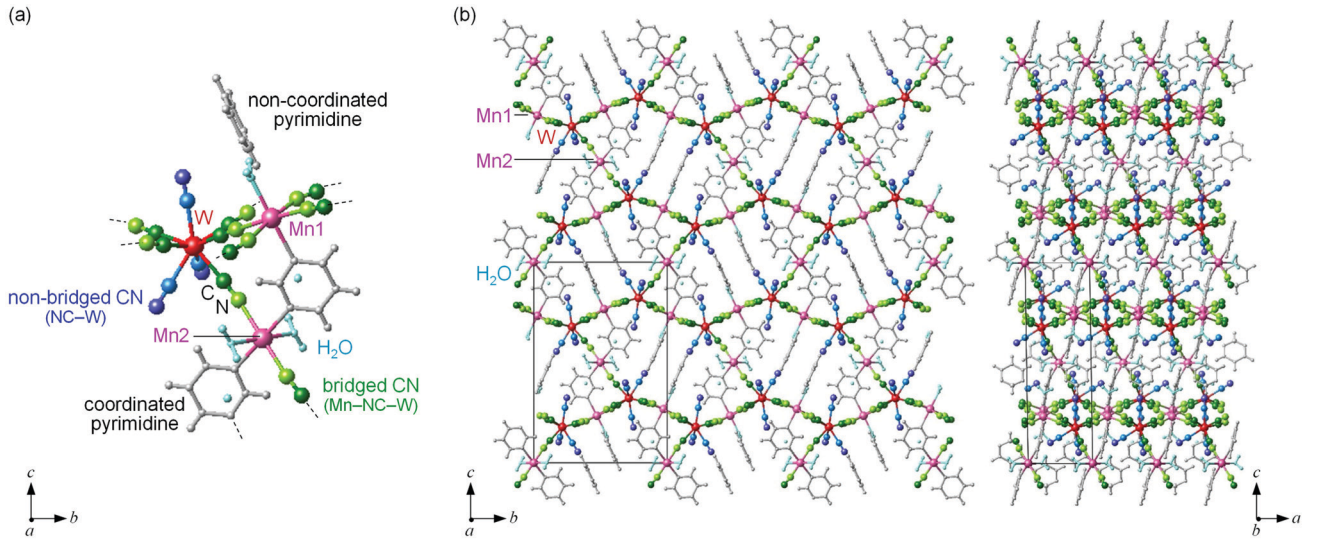

Fig. 1 Crystal structure of MnW. (a) Coordination environments around Mn and W. (b) Three-dimensional crystal structures viewed along the *a* axis (left) and the *b* axis (right). Pink and red balls represent Mn and W, respectively. Green and light green balls represent C and N of the bridged cyanide (Mn–NC–W), whereas blue and dark blue represent C and N of the non-bridged cyanide (NC–W), respectively. Grey balls and sticks indicate pyrimidine molecules and light blue balls indicate water molecules.

using a Rigaku R-AXIS Rapid imaging plate area detector with graphite monochromated Mo Kα radiation. The crystal was covered with Paratone. The average correction of the diffraction data was performed in the Crystal Structure program in Rigaku. The crystal structure was solved by a direct method using SHELXS-97 and refined by the full-matrix least-squares method on F^2 with SHELXL-2016/6 on Olex 2-1.2 software (CCDC 2061511).† IR spectra were recorded on a SHIMADZU IRAffinity-1S spectrometer using CaF_2 plates as a sample holder. The temperature during the IR measurements was controlled by an Oxford Instrument MicrostatHe. Liquid paraffin was used as a thermal medium to keep thermal contact between the sample and the sample holder. For the temperature dependence plots of the IR peaks, peak separation was performed at each temperature, and the frequencies of the separated peaks were plotted.

First-principles phonon mode calculation

First-principles calculations based on density functional theory were conducted for manganese octacyanotangstate, $Mn_3[W(CN)_8]_2(pyrimidine)_4{\cdot}6H_2O$, using the MedeA-VASP (Vienna *ab initio* simulation package) 5.4.4 code[57,58] by GGA+*U*. Wave functions based on the plane waves and the potentials of the core orbitals were represented by the projector-augmented wave of Blöchl. The exchange–correlation term was evaluated by the generalized gradient approximation by Perdew, Burke, and Ernzerhof. The lattice parameters and atomic positions were optimized with an energy cut-off of 500 eV and a $3 \times 3 \times 3$ *k* mesh until satisfying a 10^{-5} eV pm^{-1} force tolerance. $2 \times 1 \times 1$ supercells of the optimized structures were used to calculate the phonon modes of $Mn_3[W(CN)_8]_2(pyrimidine)_4{\cdot}6H_2O$, which were determined by the direct method implemented in MedeA-Phonon[57,59] with 2-pm displacements using the optimized atomic positions. The *U*–*J* values for Mn and W d-states were set to 4.0 eV and 2.2 eV, respectively.

Results

Crystal structure and magnetic properties

MnW was prepared by mixing an aqueous solution of manganese chloride, cesium octacyanotungstate, and pyrimidine, as previously reported (see Methods).[54] The mid-infrared (IR) spectrum of MnW displays seven peaks around 2150–2190 cm^{-1} at room temperature, which are assigned to the CN stretching modes of Mn^{II}–NC–W^{V} or NC–W^{V} (Fig. S1, ESI†). Single-crystal X-ray structural analysis indicated that MnW has a monoclinic crystal structure in the $P2_1/n$ space group with a lattice constant of a = 7.2319(4) Å, b = 14.9477(8) Å, c = 22.4483(13) Å, and β = 90.920(6)° at room temperature (Fig. 1 and Table S1, ESI†).[60] In this compound, Mn (Mn1 and Mn2) and W are bridged by the CN ligand to form a three-dimensional network, *i.e.*, the cyanide-bridged Mn1–W zigzag layers along the *ab* plane are linked by Mn2 (Fig. 1). The coordination geometries of the Mn (Mn1 and Mn2) and W sites are pseudo-octahedron (D_{4h}) and square antiprism (D_{4d}), respectively. Mn1 is bonded by four nitrogen atoms of $[W(CN)_8]$, one nitrogen atom of the pyrimidine molecule, and one oxygen atom of the coordinated water molecule, while Mn2 is bonded by two nitrogen atoms of $[W(CN)_8]$, two oxygen atoms of the coordinated water molecules, and two nitrogen atoms of the pyrimidine molecules. Five CN ligands from $[W(CN)_8]$ are bonded to four Mn1 and one Mn2, while the three CN ligands are non-coordinated. Pyrimidine molecules coordinate Mn1 and Mn2. The coordinated pyrimidine molecules link Mn1 and Mn2, and the non-coordinated pyrimidine molecules exist in the crystal structure.

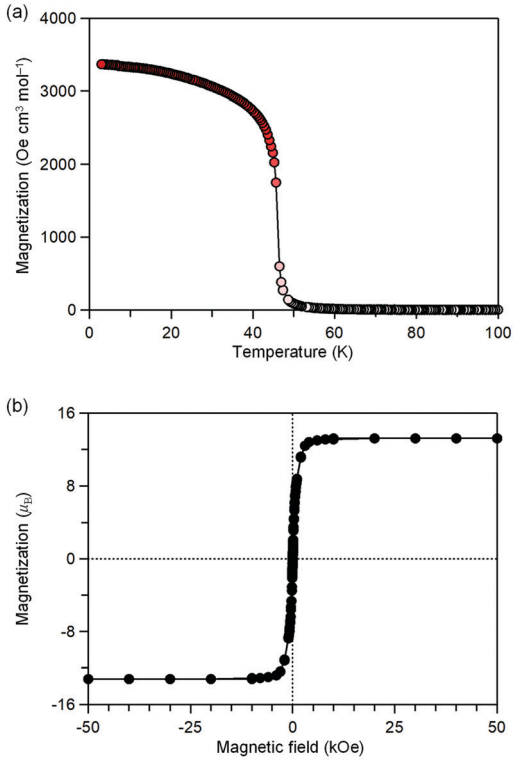

Fig. 2 Magnetic properties of MnW. (a) Magnetization *vs.* temperature plot at 20 Oe. (b) Magnetic hysteresis loop at 2 K.

MnW exhibits spontaneous magnetization below the magnetic phase transition temperature (T_C) of 47 K (Fig. 2a). The saturation magnetization (M_s) values at 2 K and 50 kOe are 13.2 μ_B (Fig. 2b and Fig. S4, ESI†). This corresponds to the theoretical M_s value of 13.0 μ_B with an antiparallel spin alignment between Mn^{II} (S_{Mn} = 5/2) and W^V (S_W = 1/2), indicating that MnW is a ferrimagnet.

Temperature dependence of the IR spectrum

The temperature dependence of the IR spectrum in the magnetic ordering temperature region was studied. Fig. 3a shows the observed IR spectra at 5 K and 60 K. Around 2150–2200 cm^{-1}, eight peaks due to the CN stretching frequency (ν) are observed. Here, the peaks are labelled as peaks 1–8 from the low energy frequency as shown in Fig. 3a.

Fig. 3b shows the peak positions of the CN stretching frequency (ν_1–ν_8) *versus* temperature (Fig. S5, ESI†). Red line indicates the peak position obtained by fitting a theoretical equation of thermal expansion due to anharmonic phonons without magnetic ordering.[61] ν_1, ν_2, and ν_3 shift towards higher frequencies below 50 K, indicating a contraction of the bonds bridged by CN, whereas ν_4, ν_5, and ν_6 shift towards lower frequencies below 50 K, indicating an expansion of the bond. ν_7 and ν_8 do not shift below 50 K. The temperature dependence of the IR spectra indicates a correlation between the phonon mode of the CN stretching and the long-range magnetic ordering.

First-principles phonon mode calculation

The phonon modes of MnW were obtained by first-principles calculations using the MedeA-Phonon (Fig. 4 and Fig. S6, S7, ESI†). The MnW has 567 optical phonon modes and 3 acoustic phonon modes. Fig. 4a show the calculated phonon density of states. The calculated transition probabilities of the optical phonon modes are shown in Fig. 4b (upper). In the region of 100–500 cm^{-1}, the phonon modes due to the symmetric bending modes and asymmetric bending modes of Mn–N≡C–W or N≡C–W, pyrimidine molecule, and water molecule exist. By

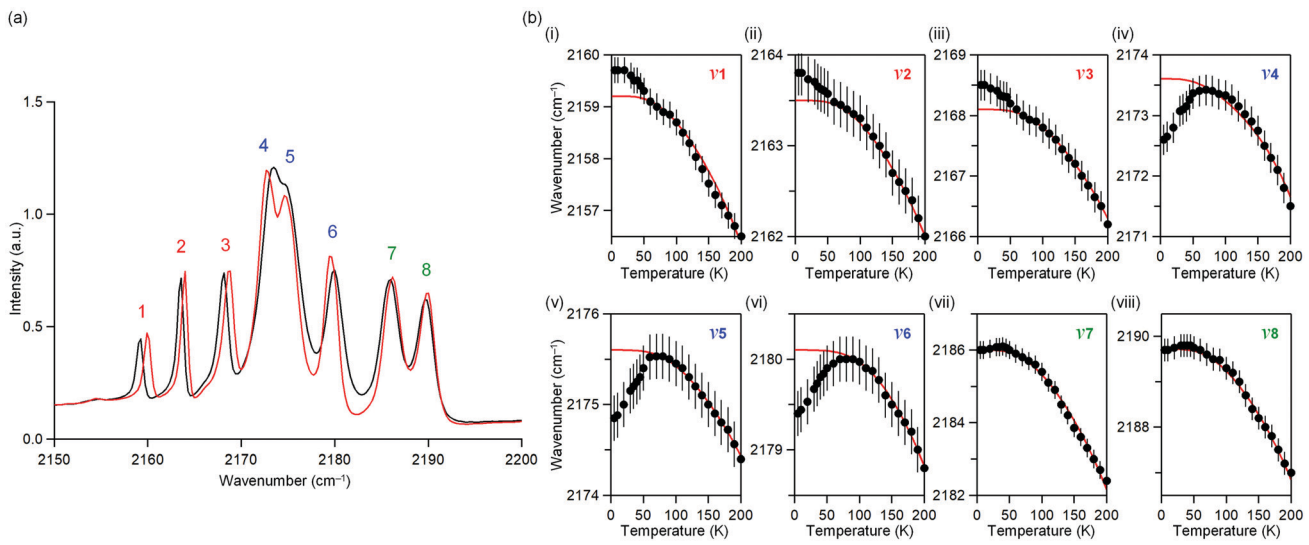

Fig. 3 Temperature dependence of the IR spectrum of MnW. (a) IR spectrum at 5 K (red) and 60 K (black). (b) IR peak frequency due to the CN stretching mode, ν_i (i = 1–8), *vs.* temperature plots. Red line indicates the peak position obtained by fitting the theoretical equation of thermal expansion[61] due to anharmonic phonons without magnetic ordering. Error bars indicate the resolution of the apparatus.

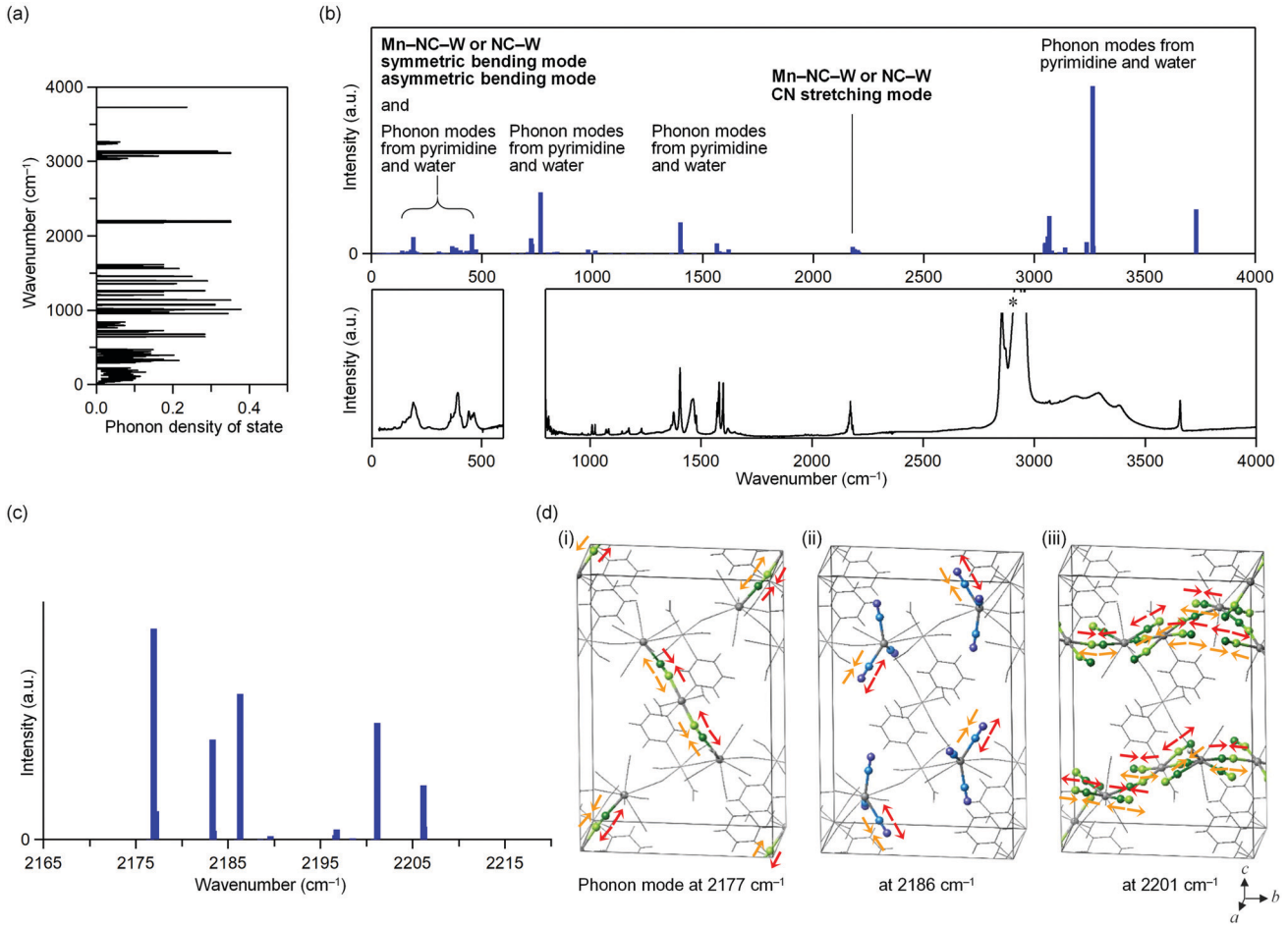

Fig. 4 First-principles phonon mode calculation of MnW. (a) Phonon density of state (DOS). (b) Calculated optical transition probabilities of the phonon modes and their assignments (upper). Blue bars denote the transition probabilities. Observed far-IR and mid-IR spectra for the regions of 0–600 cm^{-1} and 1000–4000 cm^{-1}, respectively, at room temperature (lower). Due to the influence of CaF_2 of the sample holder, the IR spectrum of the region of 600–800 cm^{-1} was not observable. Asterisk indicates the signal from liquid paraffin. (c) Calculated optical transition probabilities of the phonon modes in the region of 2155–2225 cm^{-1}. (d) Schematic illustration of the atomic movements of the phonon modes at 2177 (i), 2186 (ii), and 2201 cm^{-1} (iii). Arrows indicate the movements of the CN stretching mode. Green and light green balls represent C and N of the bridged cyanide (Mn–NC–W), whereas blue and dark blue represent C and N of the non-bridged cyanide (NC–W), respectively. Grey lines show the MnW crystal structure.

contrast, in the region of 2000–2500 cm^{-1}, the phonon modes due to the CN stretching modes of Mn–N≡C–W or N≡C–W exist. In the regions of 500–1700 and 3000–4000 cm^{-1}, phonon modes due to pyrimidine molecule and water molecule exist, respectively. From these results, in the region of 2000–2500 cm^{-1}, only the CN stretching modes are present.

Fig. 4c shows the optical transition probabilities of the CN stretching phonon modes. The strong transition probabilities are positioned at 2177, 2183, 2186, 2201, and 2206 cm^{-1}. The mode at 2177 cm^{-1} originates from the CN stretching modes of the bridged CN between Mn2 and W (Mn2–NC–W) and the bond between layers (Fig. 4d(i)). The modes at 2183 and 2186 cm^{-1} are due to the CN stretching modes of the non-bridged CN (NC–W) (Fig. 4d(ii)). The modes 2201 and 2206 cm^{-1} originate from the CN stretching modes of the bridged CN between Mn1 and W (Mn1–NC–W) and the bond in layer (Fig. 4d(iii)).

Magnetic orbitals

To study the magnetic orbitals of MnW, the discrete variable (DV)-Xα method was used to calculate the Mn–N≡C–W molecular orbitals. Mn1 and W have magnetic orbitals, *i.e.*, $Mn1d_{xy}$–$N2p_y$≡$C2p_y$–Wd_{z^2} ($Mn1d_{xy}$–W) (Fig. 5a(i)) and $Mn1d_{zx}$–$N2p_y$≡$C2p_z$–Wd_{z^2} ($Mn1d_{zx}$–W) (Fig. 5a(ii)). The overlapping orbitals in $Mn1d_{xy}$–W derived from Mn1 and W indicate an antiferromagnetic superexchange pathway. In $Mn1d_{zx}$–W, the orthogonalized orbitals derived from Mn1 and W denote a ferromagnetic superexchange pathway. For Mn2 and W, magnetic orbitals are calculated, *i.e.*, $Mn2d_{zx}$–$N2p_x$≡C–Wd_{z^2} ($Mn2d_{zx}$–W) (Fig. 5b(i)) and $Mn2d_{yz}$–$N2p_x$≡$C2p_y$–Wd_{z^2} ($Mn2d_{yz}$–W) (Fig. 5b(ii)). The overlapping orbitals in $Mn2d_{zx}$–W derived from Mn2 and W indicate an antiferromagnetic superexchange pathway. In $Mn2d_{yz}$–W, the orthogonalized orbitals derived from Mn2 and W denote a ferromagnetic the superexchange pathway. These calculations suggest that the magnetic interactions between Mn and W (Mn1–W and Mn2–W) are

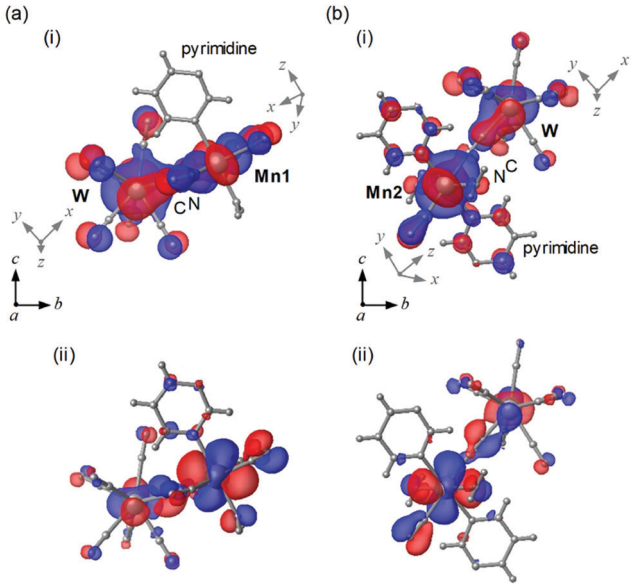

Fig. 5 Calculated magnetic orbitals for (a) Mn1 and W; (i) Mn1($3d_{xy}$)–N($2p_y$)≡C($2p_y$)–W($3d_{z^2}$) and (ii) Mn1($3d_{zx}$)–N($2p_y$)≡C($2p_z$)–W($3d_{z^2}$). (b) Mn2 and W; (i) Mn2($3d_{zx}$)–N($2p_x$)≡C–W($3d_{z^2}$) and (ii) Mn2($3d_{yz}$)–N($2p_x$)≡C($2p_y$)–W($3d_{z^2}$). Crystal structure coordinates are indicated as (*a*, *b*, *c*), whereas the coordinates for Mn and W orbits are indicated as (*x*, *y*, *z*) on the side of Mn and W, respectively. Coordinates of C and N are the same as Mn.

composed of two opposite magnetic contributions, *i.e.*, antiferromagnetic and ferromagnetic pathways.

Discussion

The first-principles calculation indicates that the phonon modes in the region of 2000–2500 cm^{-1} originate from the CN stretching modes. These modes can be classified into three types: CN stretching modes due to (i) the bridged CN between the layers (Mn2–NC–W), (ii) the non-bridged CN (NC–W), and (iii) the bridged CN in the layer (Mn1–NC–W). For the experimentally observed IR peaks below T_C, the temperature dependence is divided into three types: (i) a shift to a higher frequency (peaks 1, 2, and 3), (ii) a shift to a lower frequency (peaks 4, 5, and 6), and (iii) no shift (peaks 7 and 8) as the temperature decreases. Comparing the positions of the calculated phonon modes with the observed IR peaks suggest the following assignments: the CN stretching modes of the bridged CN between the layers (Mn2–NC–W) shift to a higher frequency, the CN stretching mode of the non-bridged CN (NC–W) shifts to a lower frequency, and the CN stretching mode of the bridged CN in the layer (Mn1–NC–W) does not shift. Because the peak shift to a higher frequency indicates contraction of the bond, (whereas the peak shift to a lower frequency indicates expansion), the shifts of the IR peaks indicate that the Mn2–NC–W bonds contract, the non-bridged NC–W bonds expand, and the Mn1–NC–W bonds are unchanged below T_C (Fig. 6). These results imply that the long-range magnetic ordering is correlated with the CN bridged bonds below T_C.[62]

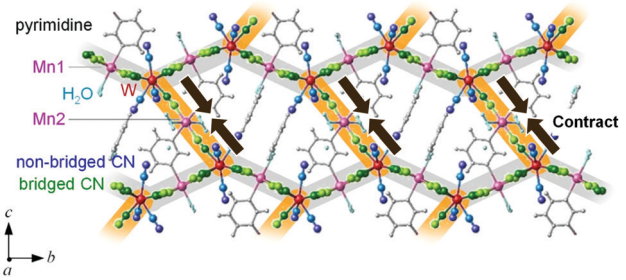

Fig. 6 Schematic image of the bond contraction for the MnW crystal. Observed shifts of the IR peaks indicate that the Mn2–NC–W bonds (highlighted by orange) contract (brown arrows), the non-bridged NC–W bonds expand, and the Mn1–NC–W bonds (highlighted by gray) are unchanged below T_C. Pink and red balls represent Mn and W, respectively. Green and light green balls represent C and N of the bridged cyanide (Mn–NC–W), whereas blue and dark blue represent C and N of the non-bridged cyanide (NC–W), respectively. Gray balls and sticks indicate pyrimidine molecules, and light blue balls indicate water molecules.

Let us consider the mechanism of contraction (or expansion) of the CN bridged bond. In MnW, bond contraction (or expansion) is observed below T_C. That is, bond contraction (or expansion) stabilizes the energy of the system below T_C. In the energy of the system, which dominates the expansion and contraction of the CN bridged bonds, there are two kinds of energies, *i.e.*, magnetic energy and elastic energy. Here, the magnetic energy is considered. Stabilization of the magnetic energy means an increase of the J value. Hence, let us consider the necessary condition for bond contraction (or expansion) from the viewpoint of the J value. The molecular orbital calculations indicate that the magnetic interactions between Mn and W are composed of two kinds of superexchange pathways: antiferromagnetic (AF) and ferromagnetic (F) pathways. When the bond length between Mn and W at T_C is set as the origin, the superexchange interaction between Mn and W is indicated as $J_{(0)}$, *i.e.*, $|J_{(0)}| = |J_{AF(0)}| - |J_{F(0)}|$. Here, the antiferromagnetic and ferromagnetic superexchange interactions are indicated as J_{AF} and J_F, respectively. When the bond length between Mn and W changes x, the magnetic interaction is described as $|J_{(0+x)}| = |J_{AF(0+x)}| - |J_{F(0+x)}|$. For contraction, $|J_{(0+x)}| > |J_{(0)}|$ should be satisfied with $x < 0$ (Fig. 7).[59–61]

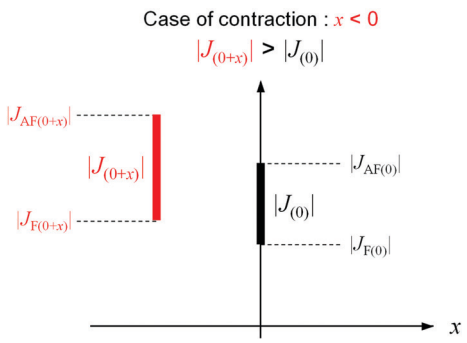

Fig. 7 Relationship between $|J_{(0+x)}|$ and $|J_{(0)}|$ in the case of bond contraction ($x < 0$).[66]

By contrast, for expansion, $|J_{(0+x)}| > |J_{(0)}|$ should be satisfied with $x > 0$. Whether the bond contracts or expands depends on the x dependence of J_{AF} and J_F. In other words, two kinds of superexchange pathways, J_{AF} and J_F, contribute to different behaviors such as contraction, lack of change, or expansion. Needless to say, the gain of the magnetic energy should exceed the loss of the elastic energy due to contraction or expansion.

The competition of the magnetic energy and the elastic energy along with the balance of the antiferromagnetic and ferromagnetic superexchange pathways can explain the contraction of the Mn2–NC–W bond. The lack of change in the Mn1–NC–W bond can be understood because the loss of elastic energy outweighs the gain of the magnetic energy. For the low frequency shift in the NC–W bond, where no magnetic interactions operate, it is attributed to the rearrangement due to the Mn2–NC–W contraction.

Conclusions

Octacyanide-bridged manganese tungstate displays a correlation between the CN stretching phonon frequency and the long-range magnetic ordering. This compound shows a relatively high T_C, isolated CN stretching modes, which do not overlap with other phonon modes such as those from organic ligands (Fig. S7, ESI†), and possesses a good stability under both vacuum and atmospheric conditions. The CN stretching frequency is closely related to the metal–cyanide bond length. The competition between the magnetic energy and elastic energy along the balance of the antiferromagnetic and ferromagnetic superexchange pathways can explain the bond contraction or the lack of change. This work demonstrates that a specific change in the phonon mode is induced by long-range magnetic ordering in flexibly structured soft matter. Compared to conventional magnets (metal magnets and metal oxide magnet), soft matter such as molecule-based magnets can exhibit various magnetic functionalities such as photomagnetism, vapor response magnetism, pressure response magnetism, spin-ionics, *etc.*[1,7,17,69–71] Fundamental knowledge about the correlation between the phonon mode (lattice vibration) and long-range magnetic ordering should help us understand the magnetic functionality and the design of future soft materials with magnetic functionality. This study is the first step in research to elucidate magnetic functionalities from the viewpoint of the correlation between the phonon mode and long-range magnetic ordering. Furthermore, this work should lead to the understanding of magnetostriction in molecular-based magnets.[72] This knowledge may be extended to the materials science field of coordination polymers.

Conflicts of interest

The authors declare no competing financial interest.

Acknowledgements

The present research was supported in part by JSPS KAKENHI (16H06521) Coordination Asymmetry, a JSPS Grant-in-Aid for Scientific Research(A) (20H00369), and a Grant-in-Aid for Scientific Research on Innovative Area Soft Crystals (17H06367). We acknowledge the Cryogenic Research Center, The University of Tokyo, the Center for Nano Lithography & Analysis, The University of Tokyo supported by MEXT, and Quantum Leap Flagship Program (Q-LEAP) by MEXT. We are grateful to M. Yoshikiyo for the technical support.

Notes and references

1 M. Verdaguer, A. Bluezen, V. Marvaud, J. Vaissermann, M. Seuleiman, C. Desplanches, A. Scuiller, C. Train, R. Garde, G. Gelly, C. Lomenech, I. Rosenman, P. Veillet, C. Cartier and F. Villan, *Coord. Chem. Rev.*, 1999, **192**, 1023–1047.
2 T. Mallah, S. Thiébaut, M. Verdaguer and P. Veillet, *Science*, 1993, **262**, 1554–1557.
3 S. Ferlay, T. Mallah, R. Ouahès, P. Veillet and M. Verdaguer, *Nature*, 1995, **378**, 701–703.
4 S. M. Holmes and G. S. Girolami, *J. Am. Chem. Soc.*, 1999, **121**, 5593–5594.
5 J. S. Miller, *Inorg. Chem.*, 2000, **39**, 4392–4408.
6 F. Renz, H. Oshio, V. Ksenofontov, M. Waldeck, H. Spiering and P. Gütlich, *Angew. Chem., Int. Ed.*, 2000, **39**, 3699–3700.
7 S. Ohkoshi, K. Arai, Y. Sato and K. Hashimoto, *Nat. Mater.*, 2004, **3**, 857–861.
8 S. S. Kaye and J. R. Long, *J. Am. Chem. Soc.*, 2005, **127**, 6506–6507.
9 X.-Y. Wang, C. Avendaño and K. R. Dunbar, *Chem. Soc. Rev.*, 2011, **40**, 3213–3238.
10 M. Clemente-León, E. Coronado, C. Marti-Gastaldo and F. M. Romero, *Chem. Soc. Rev.*, 2011, **40**, 473–497.
11 S. Ohkoshi, K. Imoto, Y. Tsunobuchi, S. Takano and H. Tokoro, *Nat. Chem.*, 2011, **3**, 564–569.
12 H.-W. Lee, R. Y. Wang, M. Pasta, S. W. Lee, N. Liu and Y. Cui, *Nat. Commun.*, 2014, **5**, 5280.
13 R. Bertoni, M. Lorenc, H. Cailleau, A. Tissot, J. Laisney, M.-L. Boillot, L. Stoleriu, A. Stancu, C. Enachescu and E. Collet, *Nat. Mater.*, 2016, **15**, 606–610.
14 A. C. Felts, A. Slimani, J. M. Cain, M. J. Andrus, A. R. Ahir, K. A. Abboud, M. W. Meisel, K. Boukheddaden and D. R. Talham, *J. Am. Chem. Soc.*, 2018, **140**, 5814–5824.
15 A. Adam, M. Poggi, E. Larquet, R. Cortès, L. Martinelli, P.-E. Coulon, E. Lahera, O. Proux, D. Chernyshov, K. Boukheddaden, T. Gacoin and I. Maurin, *Nanoscale*, 2018, **10**, 16030–16039.
16 L. Trinh, S. Zerdane, S. Mazérat, D. Dragoe, C. Herrero, E. Riviere, L. Catala, M. Cammarata, E. Collet and T. Mallah, *Inorg. Chem.*, 2020, **59**, 13153–13161.
17 S. Ohkoshi, K. Nakagawa, K. Tomono, K. Imoto, Y. Tsunobuchi and H. Tokoro, *J. Am. Chem. Soc.*, 2010, **132**, 6620–6621.

18 J.-P. Launay and M. Verdaguer, *Electrons in Molecules: From Basic Principles to Molecular Electronics*, Oxford Univ. Press, Oxford, 2017.
19 W. D. Griebler and D. Babel, *Z. Naturforsch. B*, 1982, **87**, 832–837.
20 S. Ohkoshi, T. Iyoda, A. Fujishima and K. Hashimoto, *Phys. Rev. B: Condens. Matter Mater. Phys.*, 1997, **56**, 11642–11652.
21 Ø. Hatlevik, W. E. Buschmann, J. Zhang, J. L. Manson and J. S. Miller, *Adv. Mater.*, 1999, **11**, 914–918.
22 S. Ohkoshi, Y. Abe, A. Fujishima and K. Hashimoto, *Phys. Rev. Lett.*, 1999, **82**, 1285–1288.
23 A. L. Goodwin, K. W. Chapman and C. J. Kepert, *J. Am. Chem. Soc.*, 2005, **127**, 17980–17981.
24 A. Bleuzen, C. Lomenech, V. Escax, F. Villain, F. Varret, C. Cartier dit Moulin and M. Verdaguer, *J. Am. Chem. Soc.*, 2000, **122**, 6648–6652.
25 E. Coronado, M. C. Gimenez-Lopez, G. Levchenko, F. M. Romero, V. Garcia-Baonza, A. Milner and M. Paz-Pasternak, *J. Am. Chem. Soc.*, 2005, **127**, 4580–4581.
26 H. Tokoro, K. Nakagawa, K. Imoto, F. Hakoe and S. Ohkoshi, *Chem. Mater.*, 2012, **24**, 1324–1330.
27 S. Ohkoshi, M. Yoshikiyo, A. Namai, K. Nakagawa, K. Chiba, R. Fujiwara and H. Tokoro, *Sci. Rep.*, 2017, **7**, 8088.
28 H. Tokoro, A. Namai, M. Yoshikiyo, R. Fujiwara, K. Chiba and S. Ohkoshi, *Sci. Rep.*, 2018, **8**, 63.
29 P. Gütlich, Y. Garcia and T. Woike, *Coord. Chem. Rev.*, 2001, **219**, 839–879.
30 O. Sato, S. Hayami, Y. Einaga and Z.-Z. Gu, *Bull. Chem. Soc. Jpn.*, 2003, **76**, 443–470.
31 H. Tokoro and S. Ohkoshi, *Dalton Trans.*, 2011, **40**, 6825–6833.
32 J. M. Herrera, V. Marvaud, M. Verdaguer, J. Marrot, M. Kalisz and C. Mathonière, *Angew. Chem., Int. Ed.*, 2004, **43**, 5468–5471.
33 S. Margadonna, K. Prassides and A. N. Fitch, *J. Am. Chem. Soc.*, 2004, **126**, 15390–15391.
34 T. Mahfoud, G. Molnár, S. Bonhommeau, S. Cobo, L. Salmon, P. Demont, H. Tokoro, S. Ohkoshi, K. Boukheddaden and A. Bousseksou, *J. Am. Chem. Soc.*, 2009, **131**, 15049–15054.
35 H. Tokoro, T. Matsuda, T. Nuida, Y. Moritomo, K. Ohoyama, E. D. L. Dangui, K. Boukheddaden and S. Ohkoshi, *Chem. Mater.*, 2008, **20**, 423–428.
36 E. Coronado, M. Makarewicz, J. P. Prieto-Ruiz, H. Prima-Garcia and F. M. Romero, *Adv. Mater.*, 2011, **23**, 4323–4326.
37 O. N. Risset, P. A. Quintero, T. V. Brinzari, M. J. Andrus, M. W. Lufaso, M. W. Meisel and D. R. Talham, *J. Am. Chem. Soc.*, 2014, **136**, 15660–15669.
38 S. Ohkoshi, S. Takano, K. Imoto, M. Yoshikiyo, A. Namai and H. Tokoro, *Nat. Photonics*, 2014, **8**, 65–71.
39 D. Pinkowicz, M. Rams, M. Mišek, K. V. Kamenev, H. Tomkowiak, A. Katrusiak and B. Sieklucka, *J. Am. Chem. Soc.*, 2015, **137**, 8795–8802.
40 E. Milin, V. Patinec, S. Triki, E.-E. Bendeif, S. Pillet, M. Marchivie, G. Chastanet and K. Boukheddaden, *Inorg. Chem.*, 2016, **55**, 11652.
41 K. Ridier, A. Bas, V. Shalabaeva, W. Nicolazzi, L. Salmon, G. Molnár, A. Bousseksou, M. Lorenc, R. Bertoni, E. Collet and H. Cailleau, *Adv. Mater.*, 2019, **31**, 1901361.
42 F. J. Luque, I. A. Kowalik, J. P. Prieto-Ruiz, M. Á. Niño, H. Prima-García, F. M. Romero, D. Arvanitis, C. Mathonière, E. Coronado, R. Miranda and J. J. de Miguel, *J. Mater. Chem. C*, 2019, **7**, 2305–2317.
43 T. Yoshida, K. Nakabayashi, H. Tokoro, M. Yoshikiyo, A. Namai, K. Imoto, K. Chiba and S. Ohkoshi, *Chem. Sci.*, 2020, **11**, 8989–8998.
44 X. Qi, S. Pillet, C. de Graaf, M. Magott, E.-E. Bendeif, P. Guionneau, M. Rouzières, V. Marvaud, O. Stefańczyk, D. Pinkowicz and C. Mathonière, *Angew. Chem., Int. Ed.*, 2020, **59**, 3117–3127.
45 T. Korzeniak, S. Sasmal, D. Pinkowicz, W. Nitek, R. Pełka, D. Czernia, O. Stefańczyk and B. Sieklucka, *Inorg. Chem.*, 2020, **59**, 5872–5882.
46 S. Chorazy, T. Charytanowicz, D. Pinkowicz, J. Wang, K. Nakabayashi, S. Klimke, F. Renz, S. Ohkoshi and B. Sieklucka, *Angew. Chem., Int. Ed.*, 2020, **59**, 15741.
47 M. Magott, M. Reczyński, B. Gaweł, B. Sieklucka and D. Pinkowicz, *J. Am. Chem. Soc.*, 2018, **140**, 15876.
48 O. Kahn, *Molecular Magnetism*, Wiley-VCH, Germany, 1993.
49 K. W. Chapman, P. J. Chupas and C. J. Kepert, *J. Am. Chem. Soc.*, 2005, **127**, 15630–15636.
50 J. S. Miller and A. J. Epstein, *Angew. Chem., Int. Ed. Engl.*, 1994, **33**, 385–415.
51 A. J. Banister, N. Bricklebank, I. Lavender, J. M. Rawson, C. I. Gregory, B. K. Tanner, W. Clegg, M. R. J. Elsegood and F. Palacio, *Angew. Chem., Int. Ed. Engl.*, 1996, **35**, 2533–2535.
52 R. Jain, K. Kabir, J. B. Gilroy, K. A. R. Mitchell, K. Wong and R. G. Hicks, *Nature*, 2007, **445**, 291–294.
53 C. Train, R. Gheorghe, V. Krstic, L. M. Chamoreau, N. S. Ovanesyan, G. L. J. A. Rikken, M. Gruselle and M. Verdaguer, *Nat. Mater.*, 2008, **7**, 729–734.
54 T. Kashiwagi, S. Ohkoshi, H. Seino, Y. Mizobe and K. Hashimoto, *J. Am. Chem. Soc.*, 2004, **126**, 5024–5025.
55 C. R. Dennis, A. J. van Wyk, S. S. Basson and J. G. Leipoldt, *Transition Met. Chem.*, 1992, **17**, 471–473.
56 MnW can be expressed by the following formula: $[\{Mn\ (pyrimidine)(H_2O)\}_2\{Mn(H_2O)_2\}\{W(CN)_8\}_2](pyrimidine)_2 \cdot 2H_2O$.
57 MedeA 2.22.3, MedeA-Phonon 2.0 and MedeA-VASP 5.4.4, Materials Design Inc., San Diego CA, USA, 2018.
58 G. Kresse and J. Furthmüller, *Phys. Rev. B: Condens. Matter Mater. Phys.*, 1996, **54**, 11169.
59 K. Parlinski, Z. Q. Li and Y. Kawazoe, *Phys. Rev. Lett.*, 1997, **78**, 4063–4066.
60 The results of the TGA measurement (Fig. S2, ESI†) and the PXRD pattern with the Rietveld analysis (Fig. S3, ESI†) indicate the high purity and homogeneous character of MnW.
61 F. Sayetat, P. Fertey and M. Klessler, *J. Appl. Crystallogr.*, 1998, **31**, 121–127.

62 Generally, the values of the superexchange interaction in a cyanide-bridged complex magnet range between less than 1 to several cm^{-1} (*ca.* $\sim 5\ cm^{-1}$).[1,11,63–65] The observed shift of the CN stretching frequency is *ca.* $\sim 1\ cm^{-1}$, a reasonable value of the frequency shift.
63 S. Ohkoshi, Y. Abe, A. Fujishima and K. Hashimoto, *Phys. Rev. Lett.*, 1999, **82**, 1285–1288.
64 S. Ohkoshi and K. Hashimoto, *J. Am. Chem. Soc.*, 1999, **121**, 10591–10597.
65 H. Tokoro, S. Ohkoshi, T. Matsuda, T. Hozumi and K. Hashimoto, *Chem. Phys. Lett.*, 2004, **388**, 379–383.
66 In general, when the bond contracts and the hybridization of nearest-neighbor orbitals becomes stronger, the electronic transition between the orbitals is promoted, so that the exchange interaction J between spins, represented by the overlap integral between the orbitals, becomes stronger.[67,68] In contrast, when the bond expands and the hybridization between nearest-neighbor orbitals weakens, the electronic transition between the orbitals is suppressed, that the J becomes weak.
67 M. Mochizuki, M. Kobayashi, R. Okabe and D. Yamamoto, *Phys. Rev. B*, 2018, **97**, 060401(R).
68 M. Kobayashi and M. Mochizuki, *Phys. Rev. Mater.*, 2019, **3**, 024407.
69 W. Kosaka, K. Yamagishi, J. Zhang and H. Miyasaka, *J. Am. Chem. Soc.*, 2014, **136**, 12304–12313.
70 L. Egan, K. Kamenev, D. Papanikolaou, Y. Takabayashi and S. Margadonna, *J. Am. Chem. Soc.*, 2006, **128**, 6034–6035.
71 D. Pinkowicz, M. Rams, M. Mišek, K. V. Kamenev, H. Tomkowiak, A. Katrusiak and B. Sieklucka, *J. Am. Chem. Soc.*, 2015, **1237**, 8795–8802.
72 A. Lappas, A. S. Wills, M. A. Green, K. Prassides and M. Kurmoo, *Phys. Rev. B: Condens. Matter Mater. Phys.*, 2003, **67**, 144406.

